Diabetic Complications Consortium

Application Title:

Noninvasive evaluation of diabetic nephropathy using magnetization transfer MRI.

Principal Investigator:

Takamune Takahashi MD, PhD.
Vanderbilt University School of Medicine

1. Project Accomplishments:

In this study, we evaluated the ability and utility of magnetization transfer (MT) MRI in assessing renal fibrosis in diabetic nephropathy (DN), using db/db eNOS -/- strain, a mouse model of progressive DN. To this end, first we tested four MT-MRI protocols (MTR vs. qMT, low vs. high resolution), optimized, and established the qMT method for mouse kidney imaging. Second, we have collected qMT data from WT (N=20) and db/db eNOS-/- (15-14 wks, N=14) kidneys. After imaging, we also histologically assessed renal fibrosis in these kidneys by picrosirius red stain and collagen IV immunostain and subsequent computational analysis. Finally, we examined the correlation between qMT (pool size ratio, PSR) values and histologically detected fibrosis area. However, the mean PSR values did not correlate with histological quantification of renal fibrosis. Since renal fibrosis is generally accompanied by tubular dilatation and urine retention that decrease the PSR values, we next conducted the threshold analysis, measuring abnormally high PSR area. As a result, we found that abnormally high PSR area (% area) detected by the threshold analysis is well correlated with histological fibrosis area. Based on these results, we conclude that renal fibrosis in DN can be noninvasively assessed with qMT-MRI technique with threshold PSR analysis.

2. Specific Aims:

Specific Aim: Optimize and establish the qMT protocol for mouse kidney imaging, then examine the correlation between qMT data and histological or biochemical measures of renal fibrosis.

Results:

Establishment of qMT-MRI protocol for mouse kidney imaging: All MR images were acquired on a 7T horizontal bore imaging system. The structural imaging protocols used a field-of-view (FOV) of 34x34 mm^2. For kidney segmentation, water images (**Fig. 1a-c**) were obtained based on 3-point Dixon reconstruction (gradient echo sequence, TR =45 ms, flip angle = 35º, and multiple TEs were around 4, 4.5 and 5ms). To ensure that the same region was sampled for quantitative measures in non-invasive MRI and histological sections, qMT data were collected separately for left and right kidneys at the equatorial position for each kidney. This orientation of kidney is much easier to be defined than other orientations in histologic section. One example of

the placement of a single oblique coronal slice at the equatorial position of the kidney was shown in Figure 1. We used both axial and sagittal anatomical images (**Fig. 1a&b**) to place the equatorial coronal slice (**Fig. 1c**). The qMT data set was collected using a 2D MT-weighted spoiled gradient recalled-echo sequence (TR 24 ms, flip angle =7°, matrix size 256x256, 24 acquisitions, resoltuion = ~0.133x0.133x1 mm^3). Gaussian-shaped saturation pulses (θ_{sat} = 220° and 820°, pulse width = 10 ms) were used. The first data set was collected with 12 different RF offsets and a constant logrithmic interval ranged between 1 and 80 kHz for general quality of regional MT spectra in kidney (**Fig. 1d**). Previous qMT imaging of human brain has suggested the minimal number of RF sample points (1, 2). However, due to the motion artifacts in kidney imaging, we acquired 7 RF offsets ranged between 1 and 80 kHz at two saturation powers to ensure an accurate modeling and derivation of qMT parameters in this study (which required ~34 min of imaging time). Observed relaxation rate R_{1obs} were obtained based on images acquired with two flip angles. B_1 map was based on images acquired with two flip angles, whereas B_0 map was based on two gradient echo images (ΔTE = 2 ms).

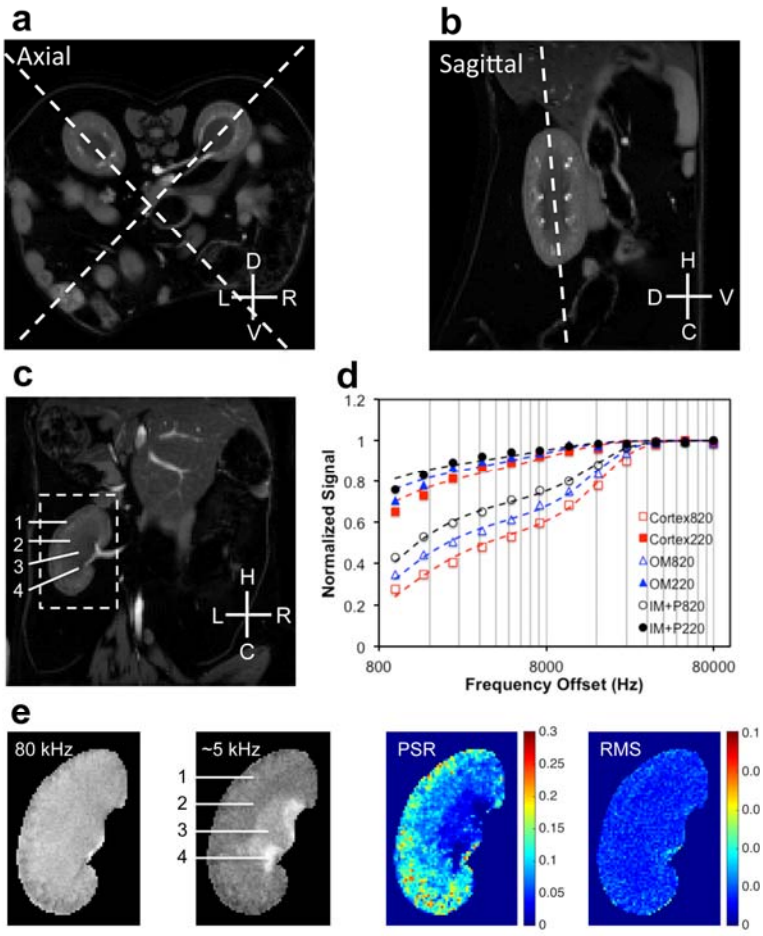

Figure 1. qMT data acquisition and quantification of murine kidney for histological comparison. (a-b) Examples showing the selection of equatorial coronal orientation for qMT data acquisition. This equatorial orientation is better for further comparison between MRI and histological results. Dashed lines indicate the selected equatorial orientations on axial or sagittal images for qMT data acquisition. L: left; R: right; D: dorsal; V: ventral; H: head; C: caudal. The axial and sagittal images are the water images from 3-point Dixon construction, and these images highlight kidneys in diabetic mice (DN mouse shown). (c) The water equatorial coronal image from 3-point Dixon reconstruction. 1-cortex, 2-outer medulla (OM), 3-inter medulla and papilla (IM+P), 4-extra renal space. (d) The example fitting of the model to regional MT data in kidney at two flip angles of θ_{sat} 220° and θ_{sat} 820°. (e) Segmented qMT images zoomed on the left kidney at RF offsets at 80 and ~5 kHz, pool size ratio (PSR) map with color-coded values, and root mean squares of the residuals (RMS) from model fitting. Example shown here is one DN mouse.

analyzed using MATLAB 2014b (The Mathworks). All intra-session images used in quantification were coregistered using a rigid registration algorithm based on mutual information (3). Kidneys were manually segmented based on T_1-weighted images (**Fig. 1c**) (4). T_{1obs} was obtained using the dual-angle approach (5).

Figure 1d compares the representative normalized signals obtained from voxels in

cortex, outer medulla (OM), and inner medulla and papilla (IM+P) of kidney at different MT saturation powers (θ_{sat} = 220° and 820°) and frequency offsets. Henkelman-Ramani's model was applied to derive qMT parameters (1, 2).

$$SI(\omega_1,\Delta f) = \frac{M_0\left(R_b[\frac{RM_{0b}}{R_a}] + R_{RFB}(\omega_{1CWFE},\Delta f,T_{2b}) + R_b + \frac{RM_{0b}}{F}\right)}{[\frac{RM_{0b}}{R_a}](R_b + R_{RFB}(\omega_{1CWFE},\Delta f,T_{2b})) + (1 + \left[\frac{\omega_{1CWFE}}{2\pi\Delta f}\right]^2 [\frac{1}{T_{2a}R_a}])(R_R \; o(\omega_{1CWFE},\Delta f,T_{2b}) + R_b + \frac{RM_{0b}}{F})} \quad (1)$$

where ***a*** and ***b*** denote the free water pool and macromolecular pool, respectively. F is the relative size of the macromolecular pool, defined as $F=M_{0b}/M_{0a}$. M_{0a} and M_{0b} are the fully relaxed values of magnetization associated with the two pools, and M_0 is the signal without MT-weighting. The continuous wave power approximation (CWPE) was applied and ω_{1CWPE} is the amplitude of the saturating field (1, 2). Δf represents the frequency offset of the MT pulse. R_{RFB} is the rate of saturation of longitudinal magnetization in pool ***b*** due to the irradiation by the amplitude defined by ω_{1CWPE} and Δf (2), which is also dependent on the transverse relaxation time of the macromolecular pool T_{2b}. A super-Lorentzian line shape is used to represent the bound pool (2). T_{2a} is the transverse time of free water pool. R is the exchange rate constant. R_a and R_b are the respective longitudinal relaxation rates. Additional constraints were imposed to determine qMT parameters. R_b was kept fixed at 1 s^{-1} as usual (1, 2, 6). Another constraint was imposed by measuring the observed longitudinal relaxation rate R_{1obs} independently, which was linked to R_a (6).

$$R_a = R_{1obs} - RM_{0b}(R_b - R_{1obs})/(R_b - R_{1obs} + \frac{RM_{0b}}{F}) \quad (2)$$

M_0, F, RM_{0b}, T_{2a} and T_{2b} were determined from the model fitting. The PSR was defined as the "F" value from the fitting. The fitting quality at each pixel was evaluated by the root mean squares (RMS) of the residuals at each RF offset. The corresponding PSR and RMS maps and selected images with MT contrast (MTC) were shown in **Figure 1e**.

T_1-weighted and MTC images were used for manual selection of ROIs (regions of interests) such as cortex, OM, IM+P, and extra-renal space for quantification (**Fig. 1c&e**). It is very challenging to distinguish cortex and outer stripe of outer medulla (OSOM) from MR images. Then in this work, the defined cortical region included both conventional renal cortex and OSOM, and OM region included only inner stripe of outer medulla (ISOM). To minimize partial volume effects, small ROIs were selected and voxels residing along the regional edges were excluded.

We tested four MT techniques (MTR, qMT etc.) and protocols and established the qMT method for mouse kidney imaging. The number of RF offsets and the resolution of qMT imaging have been optimized for detecting renal fibrosis. Multiple MRI parameters such as pool size ratio (PSR), transverse relaxation time of free water pool T_{2a}, and longitudinal relaxation R_{1obs} have been measured for WT mice (N=20). Threshold PSR values were obtained based on the regional PSR distributions (means and standard deviations) from 20 WT mice kidneys, and the regions that show significantly higher PSR was mapped in db/dbeNOS-/- kidneys (N=14).

PSR distribution and tPSR: The regions with fibrosis were selected according to their high PSR values. The normal PSR range was defined as Mean ± 2SD (standard deviation, 95%) of the normal WT mice (N=20), and regions with significantly higher PSR was defined as voxels with PSR out of this normal range. Regions with PSR higher than different threshold at Mean+2SD, Mean+3SD, or Mean+4SD were detected and percent areas of those regions in the cortex were calculated. The positive threshold PSR (tPSR) was quantified as

$$tPSR = \frac{Area\ (PSR > threshold)}{Total\ Area} \times 100\% \qquad (3)$$

The cortical PSR distributions across pixels and threshold PSR maps based on respective cortical cut-points were compared between characteristic WT and DN kidneys in **Figure 2**. In one representative normal WT kidney, the rate for pixels to show above threshold was low (tPSR < 2.5%). However, in the representative DN kidney, the distribution of PSR showed more broaden range in the cortex than that of normal WT kidney, and the rate for pixels to show above threshold increased (**Fig. 2a**). The cortical tPSR values in this DN kidney were 19.70%, 11.56%, and 6.52% for thresholds at Mean+2SD, Mean+3SD and Mean+4SD respectively (**Fig. 2b**).

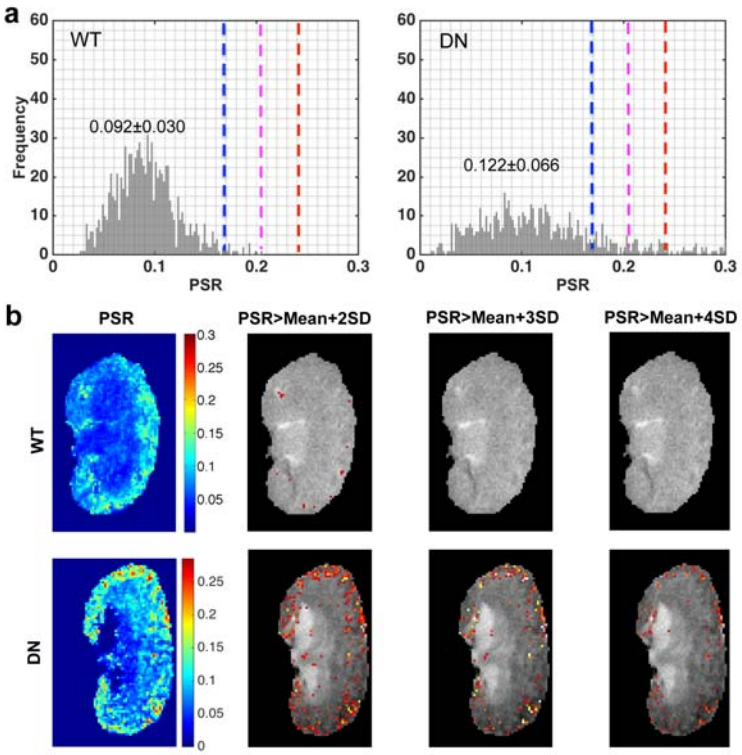

Figure 2. Comparison of PSR distributions and tPSR maps in the cortex of WT and DN kidneys. (a) PSR distributions in the cortexes of representative WT and DN kidneys. The blue, purple and red dash lines indicate Mean+2SD, Mean+3SD, and Mean+4SD of PSR in cortex respectively. The Mean and SD of cortical PSR are the statistic results from the cortex of normal WT kidneys (N=20). (b) PSR maps and threshold PSR maps that highlight the regions with significantly higher PSR values than those of normal mouse. The percent area with PSR>Mean+2SD, PSR>Mean+3SD or PSR>Mean+4SD in the total area of cortex is calculated for further comparison with histological fibrosis indexes.

Correlation of PSR measures with histological fibrosis indexes: For histological fibrosis indexes, stained slides were scanned using Leica SCN400 Slide Scanner. The positive collagen IV and positive picrosirius red areas in cortex were selected in all the corresponding sections using image analysis software (Digital Image Hub; Leica Biosystems.), with dark color in

collagen IV and red color in picrosirius red stains respectively. Then the regional fibrosis index was estimated by the area percentage of the positive pixels.

$$Positive\ collagen\ IV = \frac{Area\ (dark)}{Total\ Area} \times 100\% \qquad (4)$$

$$Positive\ picrosirius\ red = \frac{Area\ (red)}{Total\ Area} \times 100\% \qquad (5)$$

In histological section, the kidney deformation, tissue shrinking, and tissue damage could have impact on assessing global fibrosis level in IM+P and OM regions of kidney. Then we only quantified histological fibrosis indexes in cortex and OSOM for comparison. The correlations between tPSR and histological fibrosis indexes were calculated across kidneys, using the Pearson correlation function. The significance of measurement differences was evaluated using Student's t-tests.

The positive picrosirius red and collagen IV indexes showed high correlation in cortex (r = 0.874, p <0.001) across kidneys, indicating that the two histological fibrosis indexes are consistent in evaluating fibrosis occurred in cortex. To estimate the specificity of threshold tPSR for detecting fibrosis, we correlated directly the tPSR with the histological fibrosis indexes based on both collagen IV and picrosirius stains in the cortex across kidneys (**Fig. 3**). We found that tPSR was highly correlated with the degree of fibrosis (indicated by positive collagen IV and positive picrosirius red stains) in the cortex. The positive picrosirius red showed inter-kidney correlation coefficients 0.888, 0.852, and 0.735 with tPSR (p < 0.001) at Mean+2SD, Mean+3SD and Mean+4SD respectively, while positive collagen IV showed 0.887, 0.828 and 0.746 with tPSR (p < 0.001) at respective cutting points. It is of note that histological fibrosis index showed the highest correlation with tPSR at Mean+2SD. Compared to tPSR, the regional mPSR showed much weaker correlations with the histological fibrosis indexes in cortex, with *correlation coefficients* at 0.603 (p = 0.003) and 0.551 (p = 0.008) observed for collagen IV and picrosirius red stains respectively.

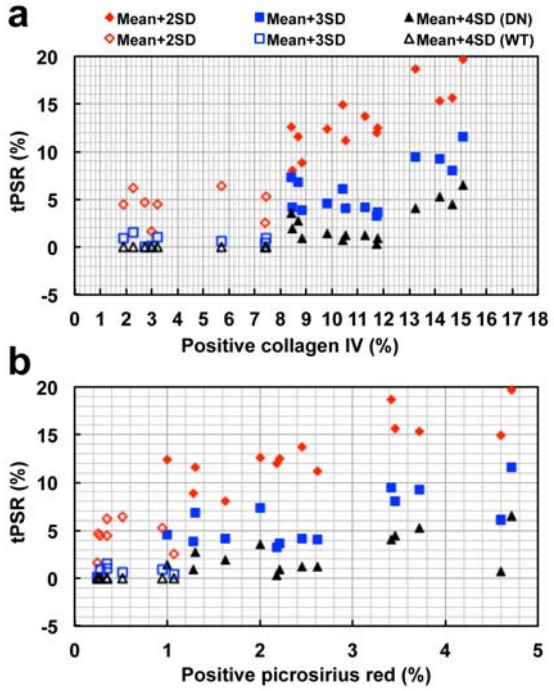

Figure 3. Correlation between tPSR and histological fibrosis indexes across kidneys. Histological fibrosis indexes were estimated using both positive collagen IV (a) and positive picrosirius red stains (b). The Non-filled markers indicate WT kidneys (N=8) and the filled markers indicated DN kidneys (N=14). Only kidneys with both MRI and histological results were included.

References

1. Ramani A, Dalton C, Miller DH, Tofts PS, and Barker GJ. Precise estimate of fundamental in-vivo MT parameters in human brain in clinically feasible times. *Magnetic resonance imaging.* 2002;20(10):721-31.
2. Cercignani M, and Barker GJ. A comparison between equations describing in vivo MT: the effects of noise and sequence parameters. *Journal of Magnetic Resonance.* 2008;191(2):171-83.
3. Pluim JPW, Maintz JBA, and Viergever MA. Mutual-information-based registration of medical images: A survey. *Ieee T Med Imaging.* 2003;22(8):986-1004.
4. Wang F, Jiang RT, Tantawy MN, Borza DB, Takahashi K, Gore JC, Harris RC, Takahashi T, and Quarles CC. Repeatability and sensitivity of high resolution blood volume mapping in mouse kidney disease. *J Magn Reson Imaging.* 2014;39(4):866-71.
5. Smith SA, Edden RA, Farrell JA, Barker PB, and Van Zijl PC. Measurement of T1 and T2 in the cervical spinal cord at 3 tesla. *Magn Reson Med.* 2008;60(1):213-9.
6. Henkelman RM, Huang XM, Xiang QS, Stanisz GJ, Swanson SD, and Bronskill MJ. Quantitative Interpretation of Magnetization-Transfer. *Magnet Reson Med.* 1993;29(6):759-66.

3. Publications:

1. Wang F, Katagiri D, Li K, Nagasaka S, Li H, Takahashi K, Wang S, Quarles CC, Zhang MZ, Gore JC, Harris RC, Takahashi T. Assessment of Renal Fibrosis in Murine Diabetic Nephropathy Using Quantitative Magnetization Transfer MRI. (Manuscript in preparation).

2. Feng Wang, Daisuke Katagiri, Ke Li, Shinya Nagasaka, Hua Li, Keiko Takahashi, Suwan Wang, C. Chad Quarles, Ming-Zhi Zhang, Raymond C. Harris, John C. Gore, Takamune Takahashi. Assessment of Renal Fibrosis in Murine Diabetic Nephropathy Using Quantitative Magnetization Transfer MRI. Proc. Int. Soc. Magn. Reson. Med., 25th, p4871, 2017.

3. Daisuke Katagiri, Feng Wang, Shinya Nagasaka, Hua Li, Suwan Wang, Keiko Takahashi, Ming-Zhi Zhang, Akira Shimizu, Raymond C. Harris, and Takamune Takahashi. Quantitative magnetization transfer imaging to evaluate renal fibrosis in mouse diabetic nephropathy. The 50th Annual Meeting of American Society of Nephrology, Chicago, IL, 2016. (Meeting Abstract)